

The Planetary System to KIC 11442793: A Compact Analogue to the Solar System

J. Cabrera¹, Sz. Csizmadia¹, H. Lehmann², R. Dvorak³, D. Gandolfi^{4,5}, H. Rauer^{1,6},
A. Erikson¹, C. Dreyer¹, Ph. Eigmüller¹ and A. Hatzes²

Received _____; accepted _____

¹Institute of Planetary Research, German Aerospace Center, Rutherfordstrasse 2, 12489 Berlin, Germany

²Thüringer Landessternwarte, 07778 Tautenburg, Germany

³Universitätssternwarte Wien, Türkenschanzstr. 17, 1180 Wien, Austria

⁴Research and Scientific Support Department, ESTEC/ESA, PO Box 299 2200 AG Noordwijk, The Netherlands

⁵INAF - Catania Astrophysical Observatory, Via S.Sofia 78, 95123 Catania, Italy

⁶Center for Astronomy and Astrophysics, TU Berlin, Hardenbergstr. 36, 10623 Berlin, Germany

ABSTRACT

We announce the discovery of 7 transiting planets around a *Kepler* target, a current record for transiting systems. Planets b, c, e and f are reported for the first time in this work. Planets d, g and h were previously reported in the literature (Batalha et al. 2013), although here we revise their orbital parameters and confirm their planetary nature. Planets h and g are gas giants and show strong dynamical interactions. The orbit of planet g is perturbed in such way that its orbital period changes by 25.7h between two consecutive transits during the length of the observations, which is the largest such perturbation found so far. The rest of the planets also show mutual interactions: planets d, e and f are super-Earths close to a mean motion resonance chain (2:3:4), and planets b and c, with sizes below 2 Earth radii, are within 0.5% of the 4:5 mean motion resonance. This complex system presents some similarities to our Solar System, with small planets in inner orbits and gas giants in outer orbits. It is, however, more compact. The outer planet has an orbital distance around 1 AU, and the relative position of the gas giants is opposite to that of Jupiter and Saturn, which is closer to the expected result of planet formation theories. The dynamical interactions between planets are also much richer.

Subject headings: planets and satellites: detection – planets and satellites: dynamical evolution and stability – planetary systems – techniques: photometric – techniques: spectroscopic

1. Introduction

Finding planetary systems similar to our own is one of the main goals of exoplanet search. It is of particular interest if such systems show planetary transits, since multiple transiting planetary systems provide crucial information for the understanding of planet formation and evolution (Ford & Gaudi 2006). Mutual dynamical interactions between planets especially require an additional effort to understand their origin and to justify their long term stability. Unfortunately, such systems are difficult to find because of the low geometrical probability for transiting planets. The satellite *Kepler* (Borucki et al. 2010) has observed the planetary system orbiting the star KIC 11442793 almost continuously for more than 4 years. The *Kepler* team has published the parameters of 3 transiting candidates around this star (Batalha et al. 2013) with the identification numbers KOI 351.01, .02, and .03. A careful analysis of the light curve with the transit detection algorithm DST (Cabrera et al. 2012) reveals the presence of 4 additional transiting planets, making this system the most populated among the transiting ones. **These 4 planets are reported here for the first time (see the results of Ofir & Dreizler 2012; Huang et al. 2013; Tenenbaum et al. 2013¹).** Considering the magnitude of the star (13.7 magnitude in SDSS r) and the characteristics of the transiting candidates, we were not able to independently confirm the planets by measuring their masses with radial velocity. However, we have performed the following steps to confirm the planetary nature of the candidates: 1) medium resolution spectra of the star were taken with the Coudé-Echelle spectrograph at the Tautenburg observatory, characterizing the host star as a solar-like dwarf; 2) the analysis of the *Kepler* photometry, including the study of the motion of the PSF centroid (Batalha et al. 2010), which does not reveal any hint of the presence of

¹while this paper was in referee process, Schmitt et al. submitted to AJ a paper with an independent characterization of this system.

contaminating eclipsing binary; 3) the analysis of the timing of the eclipses reveals that the planetary candidates are dynamically interacting one with each other; and finally 4) a stability analysis of the system with the orbital dynamics integrator *Mercury* (Chambers 1999) reveals that, for the system to be stable, all the planetary candidates must have planetary masses. Therefore, we confirm in this paper the planetary nature of the 7 candidates.

2. Stellar characterization

In order to characterize the host star, five spectra were taken on June 6 and 7, 2013, with the Coudé-Echelle spectrograph attached to the 2-m telescope at the Thüringer Landessternwarte Tautenburg. The wavelength coverage was 472-736 nm and a 2 arcsec slit provided a spectral resolving power of 32 000. The exposure time for each spectrum was 40 minutes.

The spectra were reduced using standard ESO-MIDAS packages. The reduction steps included filtering of cosmic rays, background and straylight subtraction, flat fielding using a halogen lamp, optimum extraction of diffraction orders, and wavelength calibration using a ThAr lamp. Due to the low signal-to-noise ratio (SNR) of a single spectrum it was difficult to define the local continuum. Because no radial velocity shifts between the single spectra could be found, we repeated the reduction using the co-added raw spectra. The continuum of the resulting mean spectrum was then well enough defined for a proper normalization. The SNR of the mean spectrum, measured from some almost line-free parts of the continuum, was about 19.

We used the spectral synthesis method, which compared the observed spectrum with synthetic spectra computed on a grid in atmospheric parameters. The synthetic spectra

were computed with the SynthV program (Tsymbal 1996), based on a library of atmosphere models calculated with the LLmodels code (Shulyak et al. 2004). The error estimation was done from χ^2 statistics taking all interdependencies between the different parameters into account (Lehmann et al. 2011).

The step widths of the grid were 100K in T_{eff} , 0.1 dex in $\log g$, 0.1 dex in $[M/H]$, 0.5 km s^{-1} in microturbulent velocity, and 1 km s^{-1} in $v \sin i$; where $[M/H]$ means scaled solar abundances. For the determination of $v \sin i$ we used the metal lines-rich wavelengths region 491-567 nm. For all other parameters, the wavelengths range utilized was 472-567 nm which also includes H_{β} .

Table 1 lists the results obtained from the full grid in all parameters. The large uncertainties mainly originate from the large ambiguities between the different parameters and from the low SNR of the observed spectrum. We use a compilation of empirical values of stellar parameters from (Gray 2005). Comparing our results from the full grid search with the literature data, we see that we can exclude luminosity class III stars because of the values of $\log g$ and $v \sin i$. The T_{eff} derived from spectral analysis lies, within the uncertainties, between 5 600 and 6 250K which is consistent with dwarfs of spectral type G6 to F6. Based on the measured $\log g$, we cannot determine if the star is slightly evolved. Assuming that the star is a typical main sequence star of early G-type, we can adopt a $\log g$ of 4.4, which lies within the measurement error, obtaining a better constraint on T_{eff} and a slightly higher value for the metallicity (last column of Table 1). Under this assumption, we obtain T_{eff} between 5 910 and 6 340 K, corresponding to spectral types between G1 and F6. The corresponding ranges in mass and radius are relatively small, between 1.1 and 1.3 M_{sun} and 1.1 and 1.3 R_{sun} .

2.1. Reddening and distance

We determined the interstellar extinction A_v and distance d to KIC 11442793 by applying the method described in Gandolfi et al. (2008). This technique is based on the simultaneous fit of the observed stellar colours with theoretical magnitudes obtained from the *NextGen* model spectrum (Hauschildt et al. 1999) with the same photospheric parameters as the target star. For KIC 11442793 we used SDSS, 2MASS, and WISE photometry (see Table 2 and Fig. 1). We excluded the W_3 and W_4 WISE magnitudes, as the former has a SNR of 3.5 and the latter is only an upper limit. Assuming a normal extinction ($R_v = 3.1$) and a black body emission at the stellar effective temperature and radius, we found that the star reddening amounts to $A_v = 0.15 \pm 0.10$ mag and that the distance to KIC 11442793 is $d = 780 \pm 100$ pc.

3. Light curve analysis

Kepler observations of KIC 11442793 extend for 1 340 days with a duty cycle of 82%. The light curve, shown in Figure 2, reveals that the host star is not particularly active. It barely shows hints of some variations compatible with the evolution of stellar spots on its surface, with an amplitude of 0.1%

Table 1: Derived atmospheric parameters for the star.

	full grid	$\log g$ fixed
T_{eff} (K)	$5\,930 \pm 320$	$6\,080^{+260}_{-170}$
$\log g$ (cgs)	4.0 ± 0.5	4.4 (fixed)
v_{mic} (km s $^{-1}$)	1.2 ± 0.6	1.2 ± 0.6
[M/H] (dex)	-0.17 ± 0.21	-0.12 ± 0.18
$v \sin i$ (km s $^{-1}$)	4.6 ± 2.1	4.6 ± 2.1

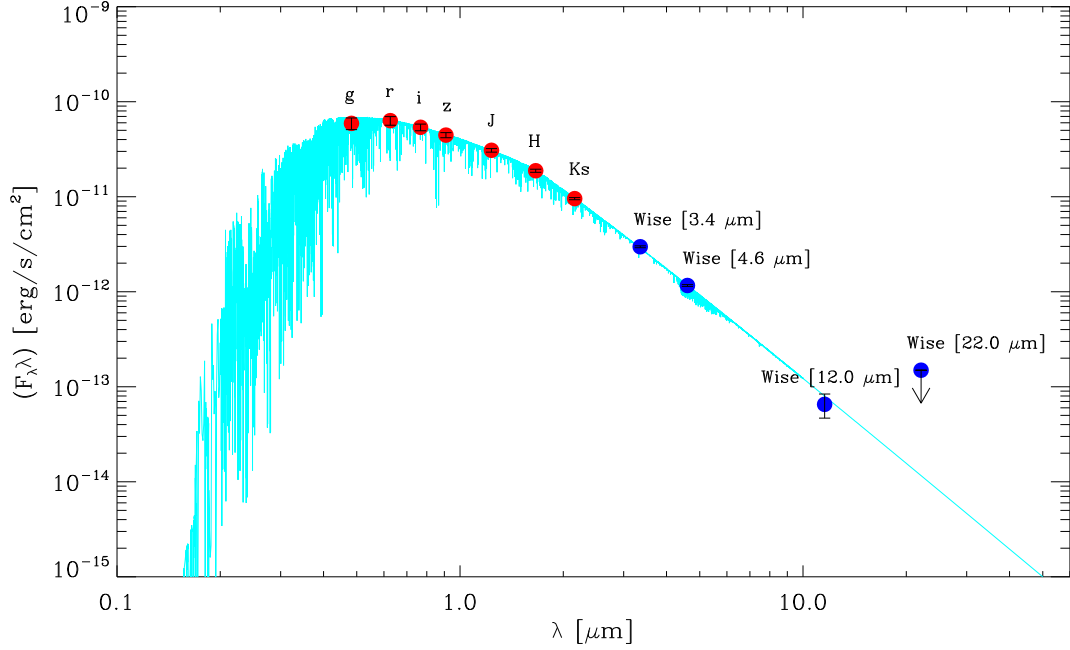


Fig. 1.— Dereddened spectral energy distribution of KIC 11442793. The optical SDSS-*g*,*r*,*i*,*z* photometry is from the *Kepler* Input Catalogue. Infrared *J*,*H*,*Ks* and *W1*, *W2*, *W3*, *W4* data are taken from the 2MASS (Cutri et al. 2003) and WISE (Wright et al. 2010) database, respectively. The *NextGen* model spectrum by Hauschildt et al. (1999) with the same photospheric parameters as KIC 11442793 and scaled to the stellar radius and distance is overplotted with a light-blue line.

Table 2: *Kepler*, GSC2.3, USNO-A2, and 2MASS identifiers of the target star. Equatorial coordinates and optical SDSS-*g*,*-r*,*-i*,*-z* photometry are from the *Kepler* Input Catalogue. Infrared *J*,*H*,*Ks* and *W1*,*W2*,*W3*,*W4* data are taken from the 2MASS (Cutri et al. 2003) and WISE (Wright et al. 2010) database, respectively.

<i>Main identifiers</i>		
<i>Kepler</i> ID	11442793	
Kepler Object of Interest	KOI 351	
GSC2.3 ID	N2EM001018	
USNO-A2 ID	1350-10067455	
2MASS ID	18574403+4918185	
<i>Equatorial coordinates</i>		
RA (J2000)	18 ^h 57 ^m 44 ^s .038	
Dec (J2000)	+49°18′18″.58	
<i>Magnitudes</i>		
Filter (λ_{eff})	Mag	Uncertainty
<i>g</i> (0.48 μm)	14.139	0.030
<i>r</i> (0.63 μm)	13.741	0.030
<i>i</i> (0.77 μm)	13.660	0.030
<i>z</i> (0.91 μm)	13.634	0.030
<i>J</i> (1.24 μm)	12.790	0.029
<i>H</i> (1.66 μm)	12.531	0.033
<i>Ks</i> (2.16 μm)	12.482	0.024
<i>W</i> ₁ (3.35 μm)	12.429	0.024
<i>W</i> ₂ (4.60 μm)	12.462	0.024
<i>W</i> ₃ (11.56 μm)	12.750	0.308
<i>W</i> ₄ (22.09 μm)	9.702 ^a	-

^aUpper limit

We have applied a detrending algorithm to treat the stellar activity optimized for the CoRoT mission (Baglin et al. 2006), but adapted to the treatment of *Kepler* data (Cabrera et al. 2012). Then we have applied the transit detection algorithm DST (Cabrera et al. 2012) to search for the periodic signature of transiting planets.

We confirm the detection of the candidates KOI 351.01, .02, and .03, previously announced (Batalha et al. 2013), and we assign them the identifications KIC 11442793 h, g, and d. We present the discovery of four additional candidates, b, c, e, and f, reported for the first time here. The ephemeris of these objects are given in Table 3. The orbital ephemeris have been calculated as follows: the transit detection algorithm DST provides preliminary values of the period, epoch, depth and duration of the transiting candidates. With this information, we first fit separately the transits of every candidate. Then we make a weighted linear fit to the epochs of the individual transits, the slope of the fit is the period and the intercept the epoch. The residuals between the linear fit and the actual position of the transits (observed minus calculated, O-C) are usually referred as transit timing variations (TTVs), which are discussed later on Section 5.

4. Planetary parameter modeling

Several planets in this system show significant transit timing variations, described in Section 5, which need to be removed before proceeding with the modeling of the planetary parameters. We use an iterative method to correct for this effect. We take a geometrical model of the transit based on the preliminary value of the planetary parameters obtained by the detection method. We use a genetic algorithm (Geem et al. 2001) to fit the value of the epoch, fixing the other transit parameters. For every trial value of the epoch, we correct for stellar activity in a region covering ten times the transit duration

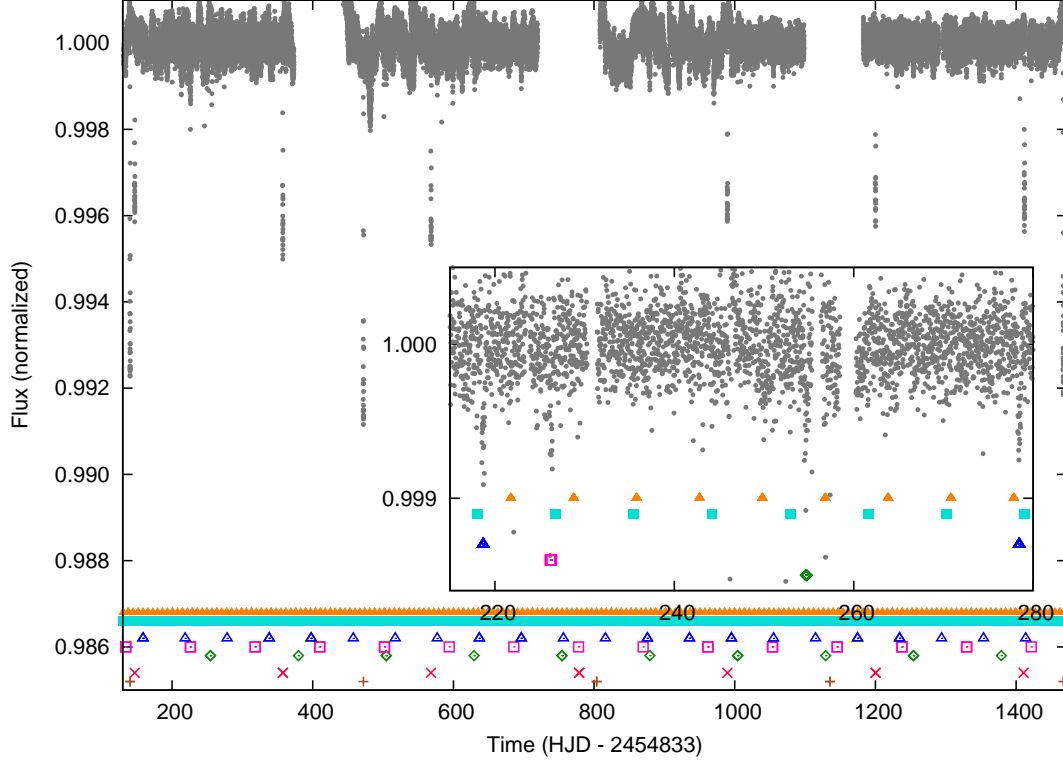


Fig. 2.— Public raw light curve of KIC 11442793. The seven sets of periodic transits are indicated with symbols of different colors: planet h with red plus-signs, planet g with red crosses, planet f with green diamonds, planet e with magenta squares, planet d with blue triangles, planet c with turquoise filled squares, and planet b with orange filled triangles. In the enlarged region the stellar variability has been subtracted to show a subset of the shallower transits.

with a second order Legendre polynomial (first order for planets b and c). The polynomial is interpolated in the expected region of the transit, to preserve the transit shape. We then fold the light curve with the obtained values of the individual epochs. This method does not converge in the case of planets b and c because of the low SNR of their transit signal. Therefore, for planets b and c we fix the period, we do not fit for the epochs, but we do apply the stellar activity correction for each individual transit described above.

A detailed description of the modeling of the planetary parameters applied here can be found in Csizmadia et al. (2011). We used the publicly available short cadence *Kepler* light curves. For candidates b, c, d, e and f we binned the light curves (we formed 2000 binned points in the $\pm 2D$ vicinity of the mid-transit, D being the transit duration), while for candidates g and h we used the original short cadence photometric points. We used the Mandel & Agol (2002) transit model. This model gives the light loss of the star due to the transit of an object as a function of their size ratio (k), of their mutual sky-projected distance (denoted by δ), and of the limb darkening coefficients of the transited star ($ld_1 = u_1 + u_2$, and $ld_2 = u_1 - u_2$).

Following Csizmadia et al. (2013) we determined the limb darkening coefficients from the light curve instead of using theoretical predictions. This fit was first applied to planet g, which has the largest transit depth i.e. the highest signal-to-noise ratio. Once obtained the values of limb darkening coefficients, we set the limb darkening coefficients at the value obtained from the fit of planet g’s transit light curve, but we allowed them to vary within the uncertainties of the determined values.

Since we do not have any radial velocity measurements, nor occultations, nor phase-curves of any of these seven planets, we had no a priori information about eccentricity and argument of periastron. Therefore we could not calculate the sky-projected distance of

the stellar and planetary centers in the usual way (e.g. Giménez 2006). Instead, we fitted the duration of the transit, the epoch (t_0), the period (P), the impact parameter (b), the planet-to-stellar radii ratio ($k = R_p/R_s$). Then the sky-projected mutual distance of the star and the planet were calculated with the formula

$$\delta \cong \sqrt{b^2 + [(1+k)^2 - b^2] \left(\frac{t-t_0}{P}\right)^2} \quad (1)$$

where t is the time. We checked the validity of this latter formula via numerical experiments and we found that in our cases it yields a very good agreement with the theoretical value in the vicinities of transits. No mutual transit event was modeled. For the optimization, a genetic algorithm process described in Csizmadia et al. (2011) was used, and the results were refined by a Simulated Annealing algorithm which was also used for the error estimation. The reported uncertainties in Table 3 are 1σ uncertainties.

We report the modeled values of k and b in Table 3 with their respective uncertainties for each of the seven candidates in the system. Once k , b , D , P became known from the modeling procedure, the value of the scaled semi-major (a/R_s) for circular orbits can then be calculated as

$$\frac{a}{R_s} = \frac{1}{\pi} \frac{P}{D} \sqrt{(1+k)^2 - b^2} \quad (2)$$

We then calculated the scaled semi-major axes for every planet in the system assuming circular orbits (see Table 3). Re-writing Kepler’s third law, we obtained for the stellar density parameter (neglecting the mass of the planet):

$$\frac{M^{1/3}}{R_s} = \left(\frac{3\pi}{GP^2}\right)^{1/3} \frac{a}{R_s} \quad (3)$$

or equivalently

$$\frac{M^{1/3}}{R_s} = \left(\frac{3}{GPD}\right)^{1/3} [(1+k)^2 - b^2]^{(3/2)} \left(\frac{1-e^2}{1+e^2-2e\sin\omega}\right)^{3/2} \quad (4)$$

We also report the density parameter derived from every candidate in Table 3. **Figures 3 to 9 show in graphical form the modelling of the photometric light curves and the model residuals for each planet.**

4.1. Analysis of the geometry of the transits

One argument supporting the hypothesis that all these planet candidates orbit the same star comes from the modeling of the planetary parameters. The inclinations and stellar densities ($M^{1/3}/R_s$) shown in Table 3 were calculated independently for each planet. They are all compatible to each other and the density is compatible with the value obtained independently for the stellar parameters in Section 2.

We can also provide another geometrical argument supporting the former hypothesis using the measured durations and periods of the transiting planets. These are obtained from a pure geometrical fit to the transits, independently of the planetary modelling techniques. This argument has previously been used in the literature to support the hypothesis that multiple candidate systems orbit actually the same star (Chaplin et al. 2013). Figure 10 shows how the transit durations distribute as a function of planetary periods. If all planets orbit the same star in circular, coplanar orbits, the transit duration D should relate to the orbital period P through Kepler’s third law:

$$D = \frac{\alpha}{\pi} P^{1/3} \sqrt{1 - \left(\frac{\cos i^2}{\alpha} P^{4/3} \right)}, \quad (5)$$

where $\alpha = (3\pi/G/\rho_s)^{1/3}$, and ρ_s is the density of the star. If D and P are in days, the best fit to the data gives a value of $\alpha = 0.23$ and $i = 90^\circ$, compatible with the values obtained from the stellar and planetary modelling. Note that the fit is not a physical solution, because all planetary orbits do not need to be exactly coplanar. However, they are compatible with all planets orbiting the same star in nearly edge-on aligned orbits, which

Table 3: Planetary parameters. Values calculated for $R_s = 1.2 \pm 0.1 R_\odot$; $R_\odot = 696\,342\text{km}$

and $R_E = 6\,378\text{ km}$.

KIC 11442793 h (KOI 351.01)		KIC 11442793 d (KOI 351.03)	
period (days)	331.60059 ± 0.00037	period (days)	59.73667 ± 0.00038
epoch (HJD - 2454833)	140.49631 ± 0.00082	epoch (HJD - 2454833)	158.9656 ± 0.0042
duration (h)	14.737 ± 0.046	duration (h)	8.40 ± 0.19
a/R_s	180.7 ± 4.7	a/R_s	56.1 ± 4.8
a (AU)	1.01 ± 0.11	a (AU)	0.32 ± 0.05
R_p/R_s	0.0866 ± 0.0007	R_p/R_s	0.0219 ± 0.0005
R_p (R_E)	11.3 ± 1.0	R_p (R_E)	2.87 ± 0.30
b	0.36 ± 0.07	b	0.28 ± 0.25
i (deg)	89.6 ± 1.3	i (deg)	89.71 ± 0.29
$M^{1/3}/R_s$	0.90 ± 0.13	$M^{1/3}/R_s$	0.88 ± 0.15
ld_1	0.348 ± 0.056	ld_1	0.371 ± 0.087
ld_2	1.03 ± 0.19	ld_2	1.04 ± 0.23
KIC 11442793 g (KOI 351.02)		KIC 11442793 c	
period (days)	210.60697 ± 0.00043	period (days)	8.719375 ± 0.000027
epoch (HJD - 2454833)	147.0364 ± 0.0014	epoch (HJD - 2454833)	139.5687 ± 0.0023
duration (h)	12.593 ± 0.045	duration (h)	4.41 ± 0.18
a/R_s	127.3 ± 4.1	a/R_s	16.0 ± 0.8
a (AU)	0.71 ± 0.08	a (AU)	0.089 ± 0.012
R_p/R_s	0.0615 ± 0.0011	R_p/R_s	0.0091 ± 0.0003
R_p (R_E)	8.1 ± 0.8	R_p (R_E)	1.19 ± 0.14
b	0.45 ± 0.10	b	0.09 ± 0.20
i (deg)	89.80 ± 0.06	i (deg)	89.68 ± 0.74
$M^{1/3}/R_s$	0.84 ± 0.14	$M^{1/3}/R_s$	0.90 ± 0.16
ld_1	0.34 ± 0.10	ld_1	0.40 ± 0.20
ld_2	0.98 ± 0.10	ld_2	1.21 ± 0.26
KIC 11442793 f		KIC 11442793 b	
period (days)	124.9144 ± 0.0019	period (days)	7.008151 ± 0.000019
epoch (HJD - 2454833)	254.704 ± 0.014	epoch (HJD - 2454833)	137.6906 ± 0.0017
duration (h)	10.94 ± 0.25	duration (h)	3.99 ± 0.15
a/R_s	86.4 ± 9.7	a/R_s	13.2 ± 1.8
a (AU)	0.48 ± 0.09	a (AU)	0.074 ± 0.016
R_p/R_s	0.0220 ± 0.0022	R_p/R_s	0.0100 ± 0.0005
R_p (R_E)	2.88 ± 0.52	R_p (R_E)	1.31 ± 0.17
b	0.35 ± 0.40	b	0.13 ± 0.32
i (deg)	89.77 ± 0.31	i (deg)	89.4 ± 1.5
$M^{1/3}/R_s$	0.84 ± 0.20	$M^{1/3}/R_s$	0.85 ± 0.21
ld_1	0.360 ± 0.068	ld_1	0.378 ± 0.060
ld_2	1.01 ± 0.18	ld_2	1.11 ± 0.20
KIC 11442793 e			
period (days)	91.93913 ± 0.00073		
epoch (HJD - 2454833)	134.3127 ± 0.0063		
duration (h)	9.71 ± 0.19		
a/R_s	74.7 ± 4.3		
a (AU)	0.42 ± 0.06		
R_p/R_s	0.0203 ± 0.0005		
R_p (R_E)	2.66 ± 0.29		
b	0.27 ± 0.22		
i (deg)	89.79 ± 0.19		
$M^{1/3}/R_s$	0.87 ± 0.15		
ld_1	0.360 ± 0.049		
ld_2	1.05 ± 0.17		

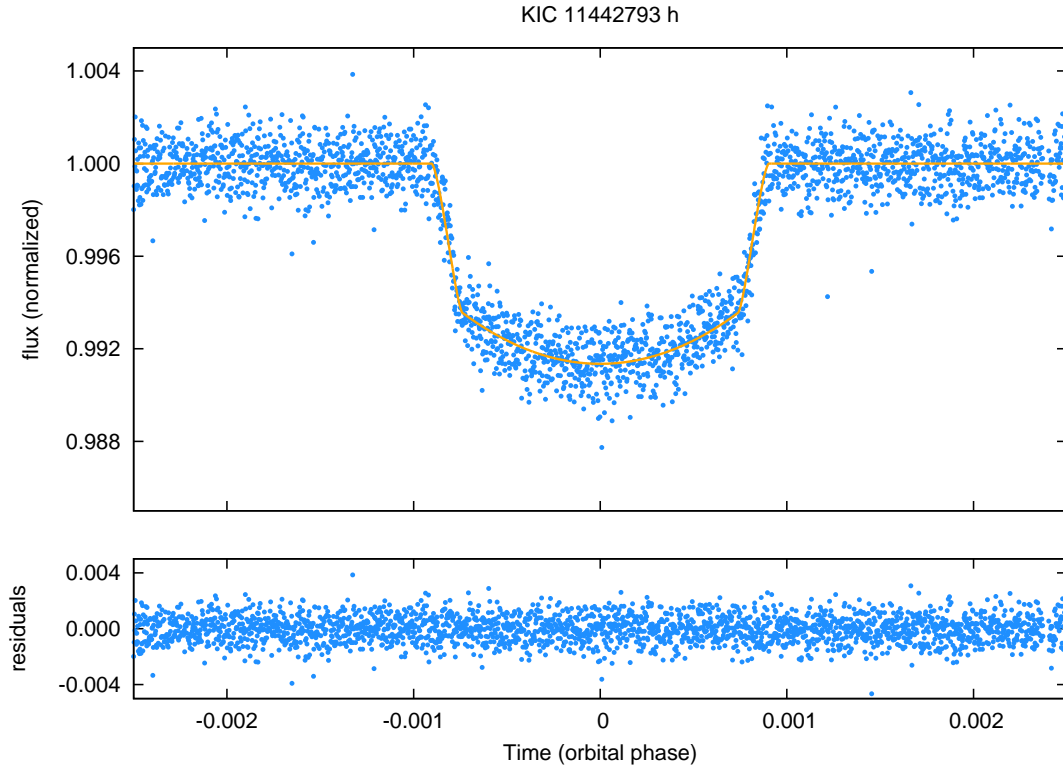


Fig. 3.— Filtered light curve of KIC 11442793 folded at the period of planet h. The orange solid line shows the light curve fit (Table 3). The lower panel shows the residuals of the light curve fit.

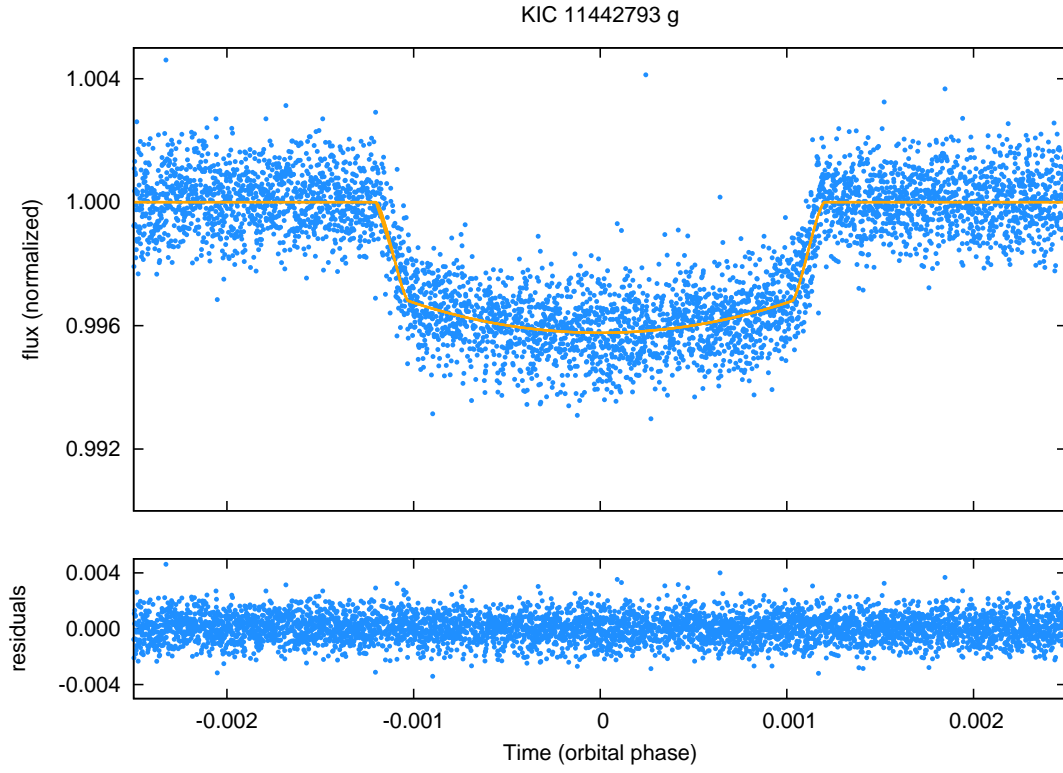


Fig. 4.— Filtered light curve of KIC 11442793 folded at the period of planet g. The orange solid line shows the light curve fit (Table 3). The lower panel shows the residuals of the light curve fit.

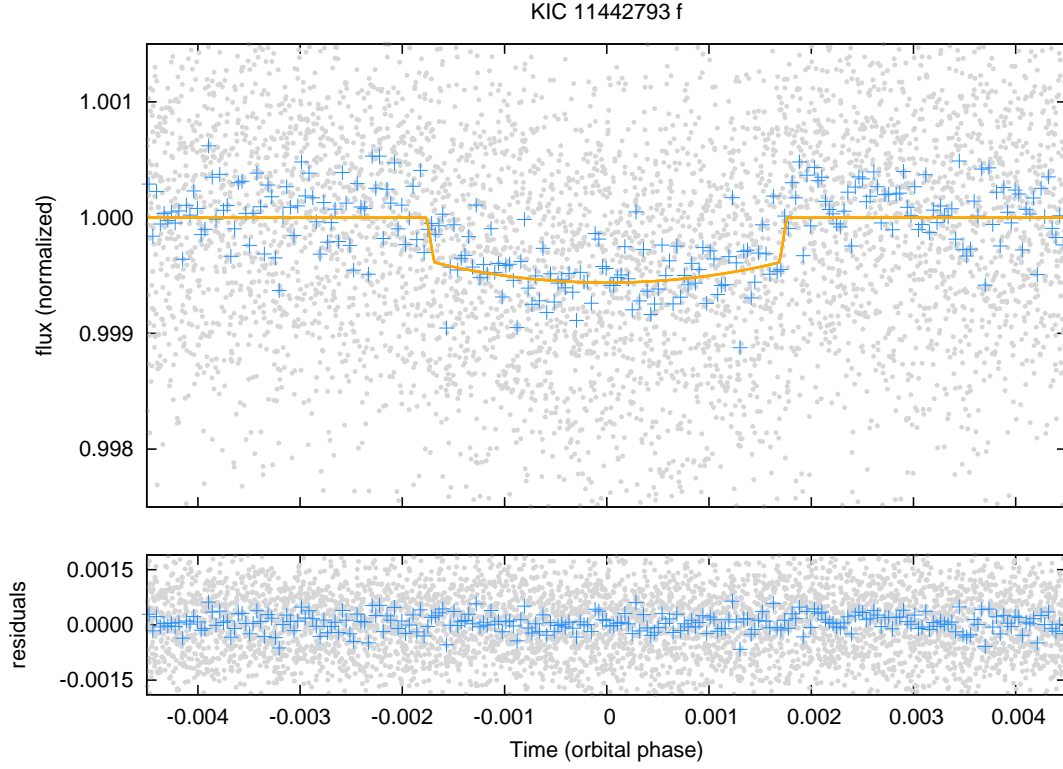


Fig. 5.— Filtered light curve of KIC 11442793 folded at the period of planet f. The light curve has been binned, to help the eye. The orange solid line shows the light curve fit (Table 3). The lower panel shows the residuals of the light curve fit.

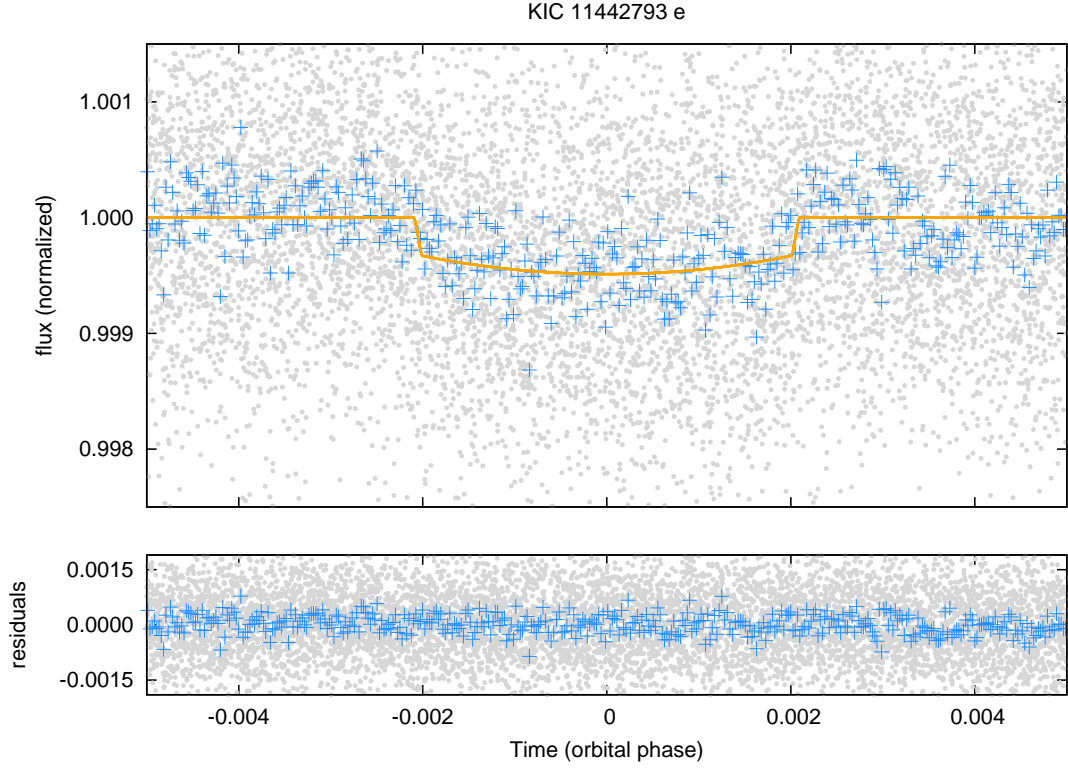


Fig. 6.— Filtered light curve of KIC 11442793 folded at the period of planet e. The light curve has been binned, to help the eye. The orange solid line shows the light curve fit (Table 3). The lower panel shows the residuals of the light curve fit.

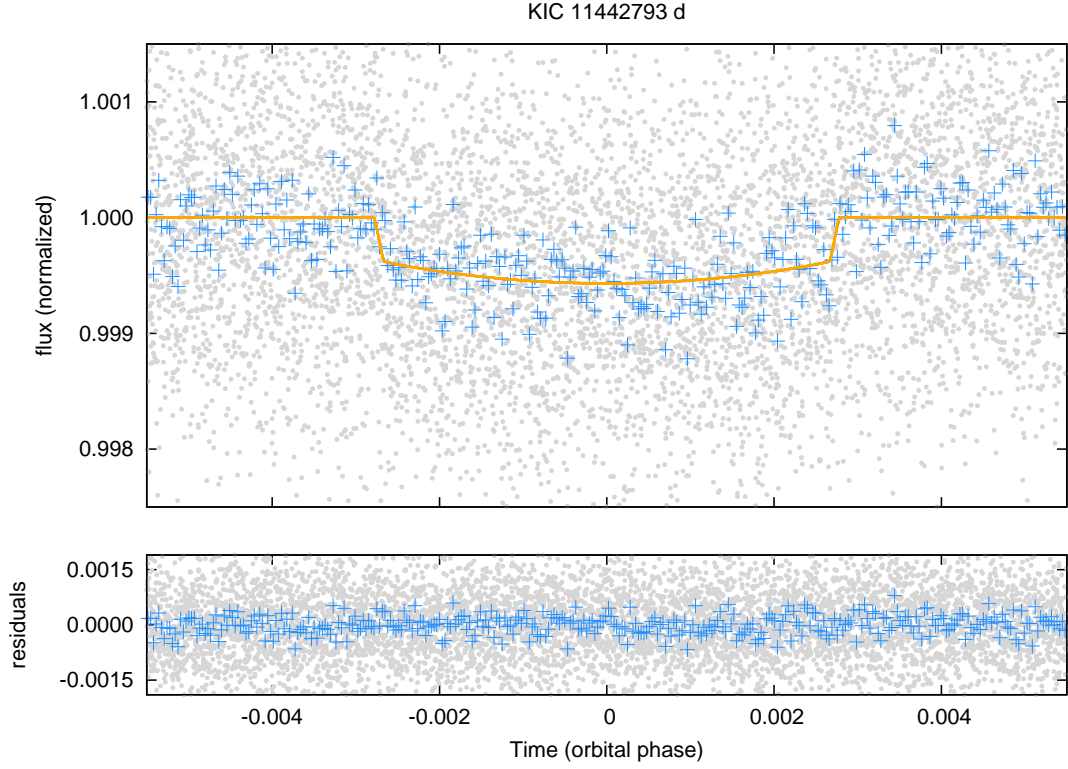


Fig. 7.— Filtered light curve of KIC 11442793 folded at the period of planet d. The light curve has been binned, to help the eye. The orange solid line shows the light curve fit (Table 3). The lower panel shows the residuals of the light curve fit.

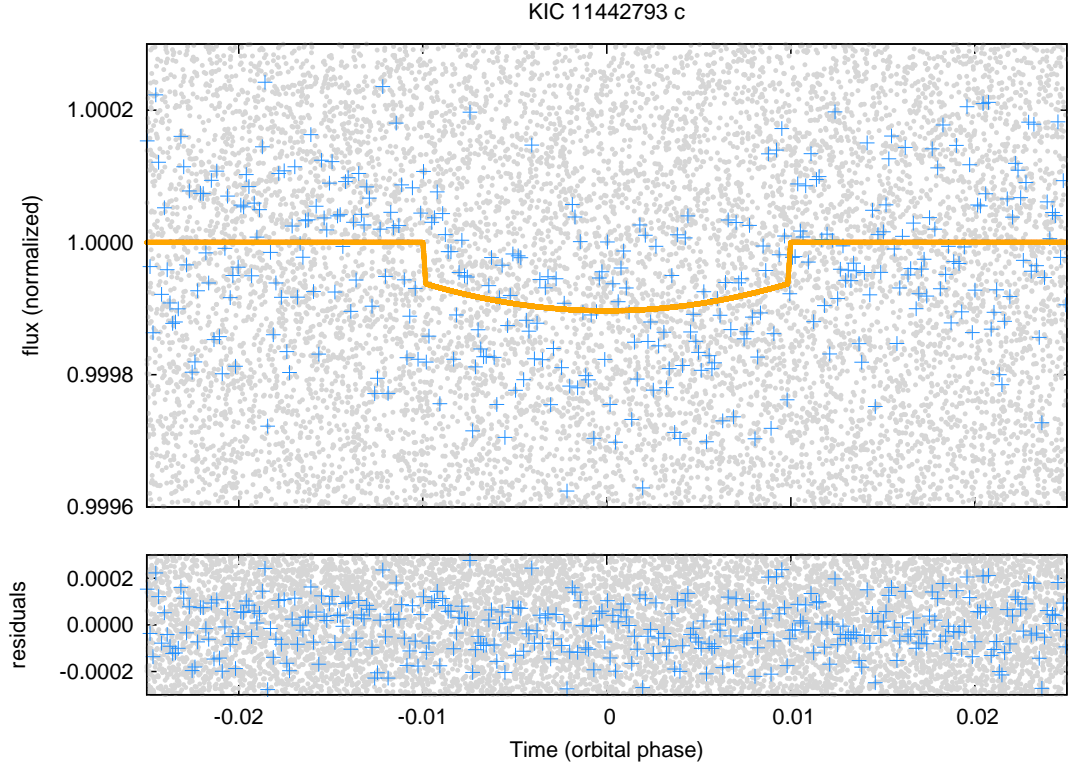


Fig. 8.— Filtered light curve of KIC 11442793 folded at the period of planet c. The light curve has been binned, to help the eye. The orange solid line shows the light curve fit (Table 3). The lower panel shows the residuals of the light curve fit.

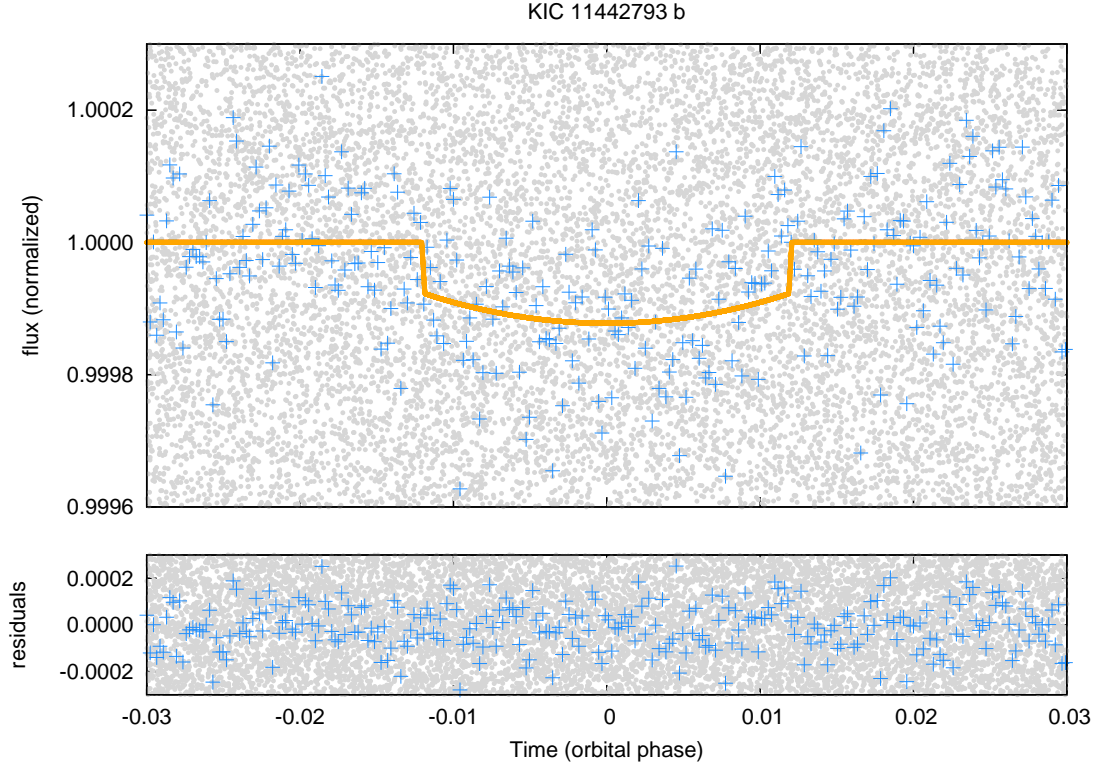


Fig. 9.— Filtered light curve of KIC 11442793 folded at the period of planet b. The light curve has been binned, to help the eye. The orange solid line shows the light curve fit (Table 3). The lower panel shows the residuals of the light curve fit.

supports our hypothesis of all planets orbiting the same star.

5. Analysis of the transit timing variations

The analysis of the transit timing variations (TTVs) has proved to be a versatile tool to confirm the planetary nature of transiting candidates (Ford et al. 2011). Typically, TTVs have amplitudes of several minutes (with some exceptional cases like KOI 142 Nesvorny et al. 2013, with an amplitude of 12h) and typically periods one order of magnitude larger than the orbital period of the planet involved (Mazeh et al. 2013).

Figure 11 shows the individual transits and Fig. 13 the O-C diagram for candidate g. The transit corresponding to epoch 7 (epoch 1 being the value provided in Table 3) has a displacement of 25.7 hours with respect to its expected position. This abrupt change is due to a change in the osculating orbital elements produced by the gravitational interaction with other objects in the system, possibly candidate h. **Most surveys of transit timing variations (TTVS) expect discovering periodic modulations of the timing perturbations (see a derivation of the searched expression in Lithwick et al. 2012 and the series of papers Ford et al. 2011, 2012a; Steffen et al. 2012a; Fabrycky et al. 2012; Ford et al. 2012b; Steffen et al. 2012b, 2013; Mazeh et al. 2013). However, non-periodic, sudden changes of the orbital elements, corresponding to irregular behaviour such as the one displayed by planet g, have been theoretically described (for example, though in a different context, Holman & Murray 2005), but we believe that we report an observational example for the first time.**

In addition to the change in the osculating elements, it is interesting to discuss separately the other transit events recorded for candidate g. The depth and the duration

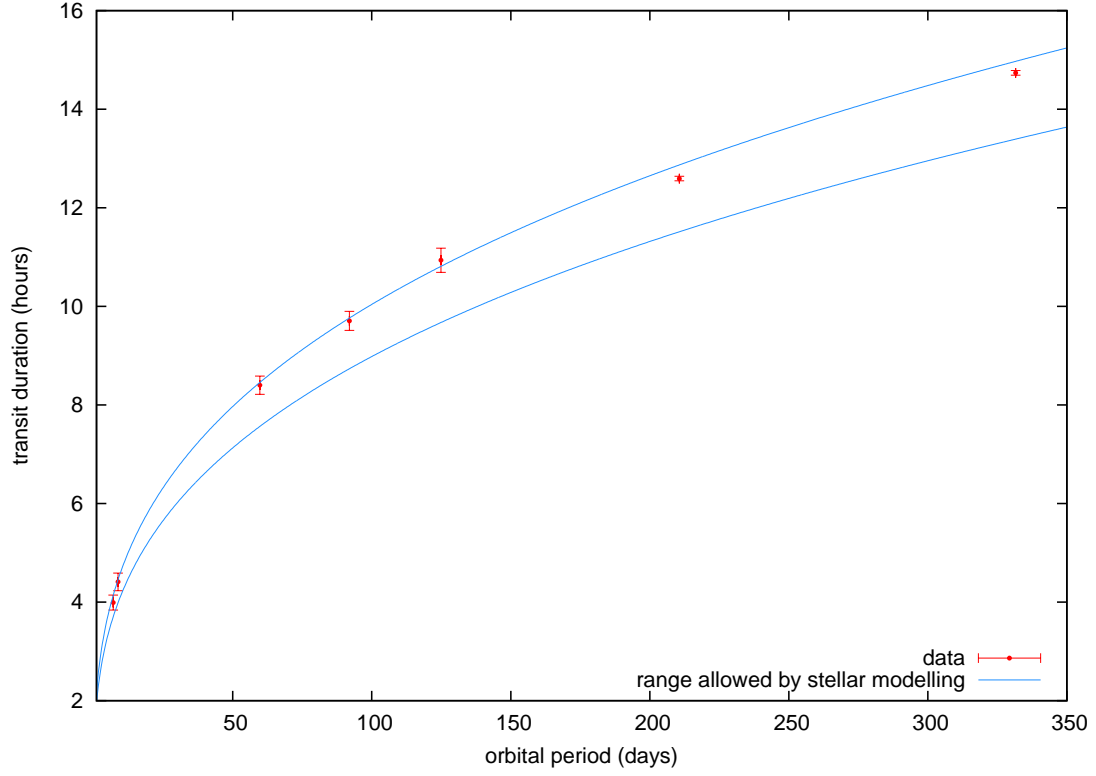


Fig. 10.— Transit duration of each planet as a function of their orbital period. The observed values are compatible with the seven planets orbiting a star whose density is that given by the stellar and planetary parameter modelling on edge-on aligned orbits. The range allowed by the modelling of the stellar parameters is indicated with the continuous blue lines.

of transit events 1, 2, and 3 changes significantly. **One can speculate that the perturbations seen around these transits are morphologically equivalent to those produced by a moon around the planet (Sartoretti & Schneider 1999; Kipping et al. 2013b). This hypothesis is further discussed in Section 7.1** We do not have enough evidence to prove that these perturbations are produced by a moon and until we have constraints on the planetary masses we cannot assess the stability of moons around candidate g. We note, just for completion, that a moon could not be responsible in any case for the abrupt change in the osculating orbital elements displayed in transit event 7. The amplitudes of the perturbations produced by moons are typically only a few seconds (Cabrera 2010; Kipping 2009a,b).

The available data set for KIC 11442793 does not allow us to do an unambiguous determination of the planetary masses from the analysis of the TTVs. Candidates b and c are too small and too close to the detection limit to measure any reliable TTV amplitude (see **Figures 17 and 18**), which is not unusual in the case of low-mass planets in compact systems (see the case of CoRoT-7b Léger et al. 2009). The TTVs of candidates d and e are compatible with zero within the limits of our current modelling (see **Figures 15 and 16**). There are only 5 transits observed from the 9 expected transits of candidate f due to some unfortunate coincidence of observing interruptions with the expected transit positions. However, there is a significant signal in the available O-C diagram, which means that candidate f is interacting dynamically with other objects in the system (see **Figure 14**).

Candidate g shows 6 transits in the available data set (expected 7) and candidate h shows 3 transits (expected 5), less than expected due to the interruptions of the photometric record (duty cycle is 82%). However, candidates g and h show both significant transit timing variations and also transit duration variations, consequently we deduce that they are interacting dynamically (see **Figures 12 and 13**). We have done a stability analysis of

the system with the orbital dynamics integrator *Mercury* (Chambers 1999). The system is only stable if candidates g and h have masses below some Jupiter units (typically, less than 5 Jupiter masses). Therefore, we conclude that g and h are planets because they interact gravitationally and their long term dynamical stability is only guaranteed if these bodies have planetary masses.

Candidates d, e, and f are close to a resonant chain 2:3:4 and the analysis of the mean motions reveal that they are probably in a Laplace resonance (see Section 6). Moreover, we know because of the significant TTV that at least candidate f is interacting dynamically with other planets (possibly g and h) in the system. The *Mercury* numerical analysis of the planetary system reveals that objects d, e, and f are in stable orbits only if those are very circular (typically, less than 3% for mass values of 10 Earth masses, representative of 2.5 Earth radii super-Earths) and planetary masses (less than the mass of Jupiter). Therefore, we conclude that these three must also be planets. Actually, the requirement of the circularity of their orbits implies that, for the system to be stable, the mean motion resonance has to play a role to guarantee the survival of the system.

We did not see any sign that candidates b and c interact dynamically with the other planets in the system because the low SNR of the transit light curves. However, the fact that their signal appears in a multiple transiting system and that their periods are within 0.5% of the 4:5 mean motion resonance speaks in favor of these two objects belonging to the same system. The *Mercury* numerical analysis reveals that their orbits are relatively stable if the objects have planetary masses.

Complementary to the numerical study, we have checked the mutual orbital distances between planets in units of their mutual Hill sphere radius (see below), a convenient method to assess the stability of multiple systems in circular, coplanar orbits (Lissauer et al. 2011b). The closest pair is g-h, separated by 4.6 Hills radii. The necessary separation for a pair to

be stable is around $3.5R_{Hill}$.

6. Dynamical study

According to their sizes, the planets h and g are potentially gas giants and their period ratio is within 1.6% of the mean motion resonance 5:8.

The planets d, e, and f have the typical sizes of super-Earths (between 2 and 3 Earth radii) and their periods are close to a chain ratio 2:3:4. The argument

$$\phi = 2\pi \left(\frac{1}{P_d} - \frac{3}{P_e} + \frac{2}{P_f} \right) \quad (6)$$

has a value of only 0.0008, indicating that the three objects could be in a Laplace resonance.

The planets b and c have radii below 1.4 Earth radius. Their period ratios are within 0.5% of the 4:5 mean motion resonance.

This exoplanetary systems needs to be seen as a very complex example where different resonances act. Seen as separated subsystems for the planets b and c, as well as d, e and f they are in a stable state even taking into account moderate eccentricities ($e \sim 0.1$). According to the Hill radii in fact the system seems to be to very 'safe' for small eccentricities. We show in Table 4 the Hill radii separating the planet pairs (for $e=0$).

The picture is completely different for the two more massive planets g and h than for the other pair b and c, and the triple d, e and f. The close resonance 8:5 for planet g and h is not so important as the secular behaviour of the two planets which are close to a 1:1 resonance with respect to their perihelions ($P_{sec} \sim 13\,000$ years). From a first estimate (Fig. 19) one can conclude that the pair planet h–g could be stable up to an eccentricity of $e \leq 0.1$. In Figure 19 we show the aphelion and perihelion positions of the five outer planets (we added the respective Hill radii $r_{Hill} = a_{\text{planet}}(M_{\text{planet}}/M_{\text{star}})^{1/3}$). According to this

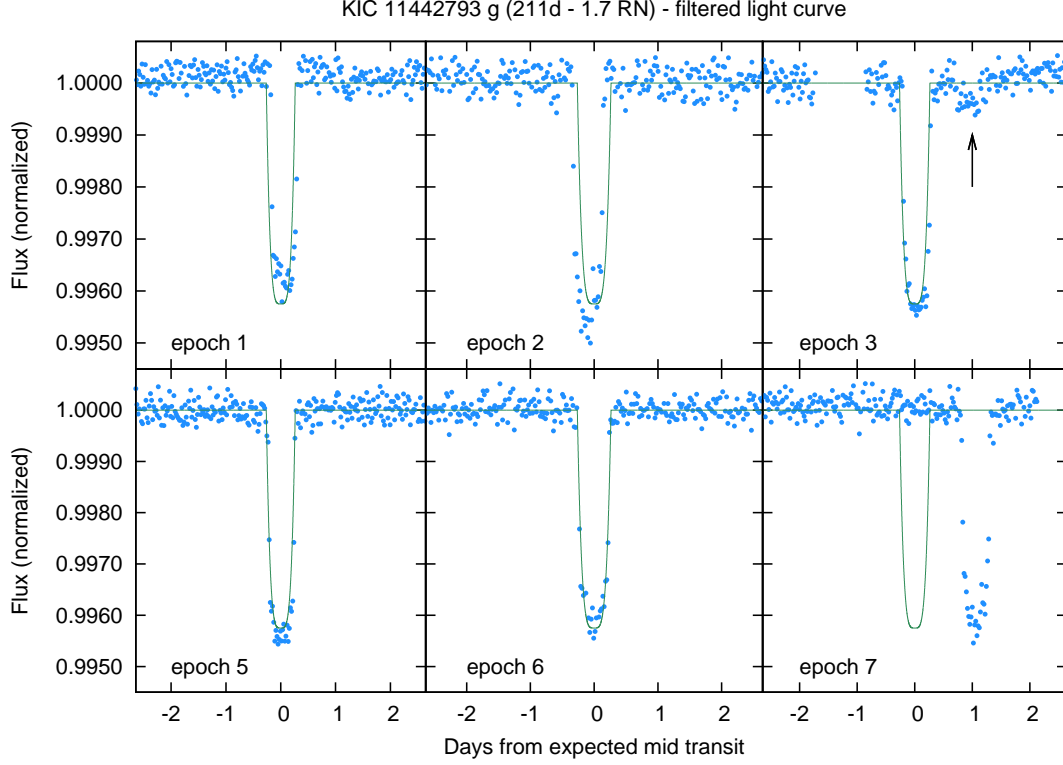


Fig. 11.— Individual observed transit events of planet g and the expected position of those transits assuming a constant period, marked with a line. Note the irregularities in the transit depth and duration at epochs 1 and 2 and the displacement from the expected position of epoch 7. The additional transit like event marked with an arrow close to epoch 3 is discussed in the text.

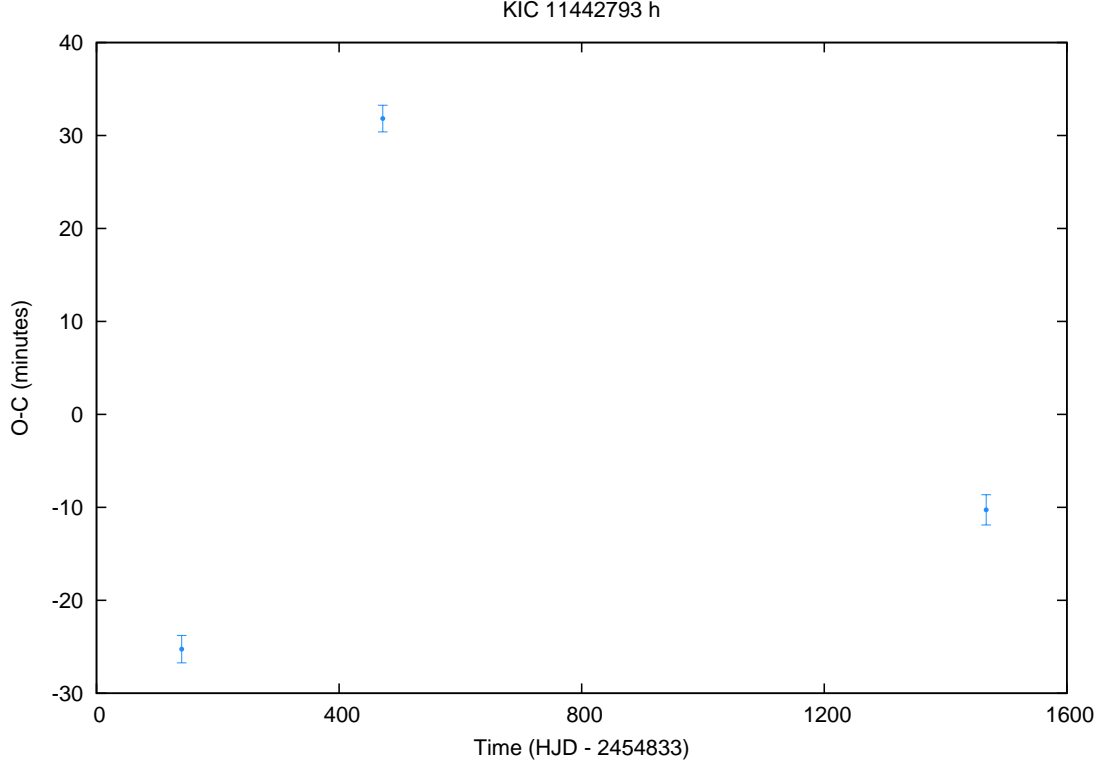


Fig. 12.— Transit timing variations of planet h. Observed mid-times of planetary transits (O) minus calculated linear ephemeris (C) are plotted with 1σ uncertainties.

Table 4: Separation in Hill radii (R_H) of the different planet pairs.

separation	a_{planet_1}	a_{planet_2}	Hill radius [AU]	separation [R_H]
h–g	0.93759	0.69275	0.05263	5
g–f	0.69275	0.48900	0.01947	10
f–e	0.48900	0.39866	0.01167	8
e–d	0.39866	0.29921	0.00918	11
d–c	0.29921	0.08290	0.00435	50
c–b	0.08290	0.07167	0.00136	8

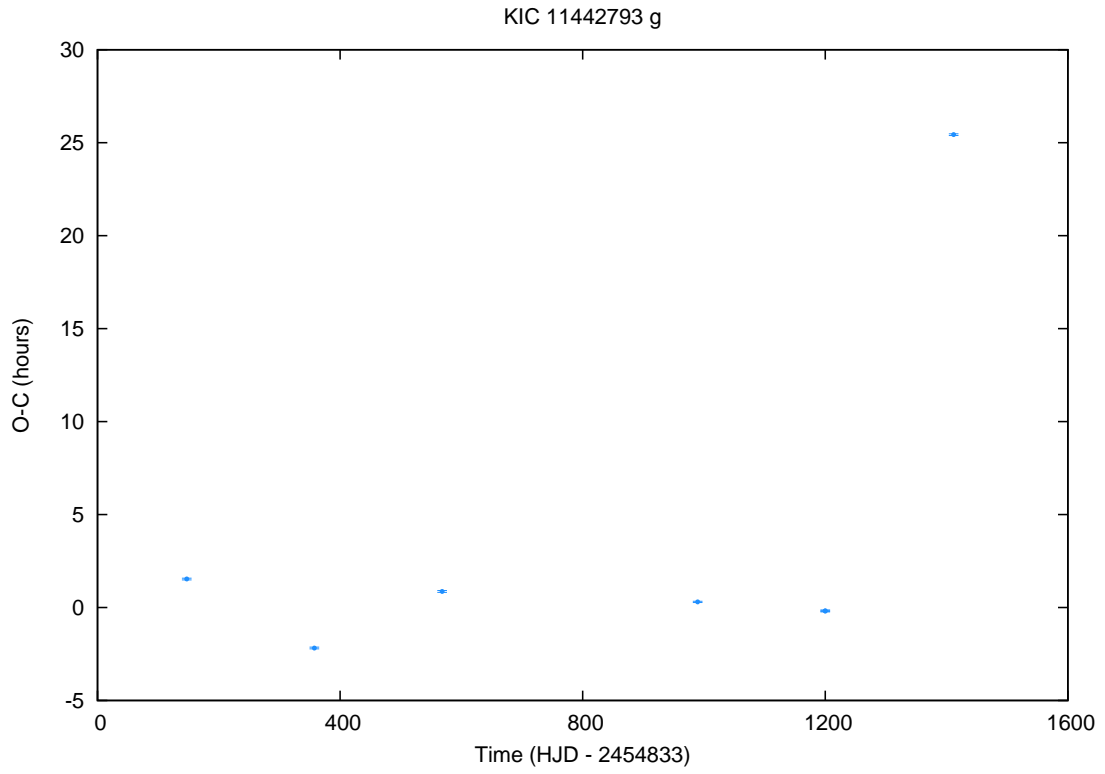


Fig. 13.— Transit timing variations of planet g. Observed mid-times of planetary transits (O) minus calculated linear ephemeris (C) are plotted with 1σ uncertainties.

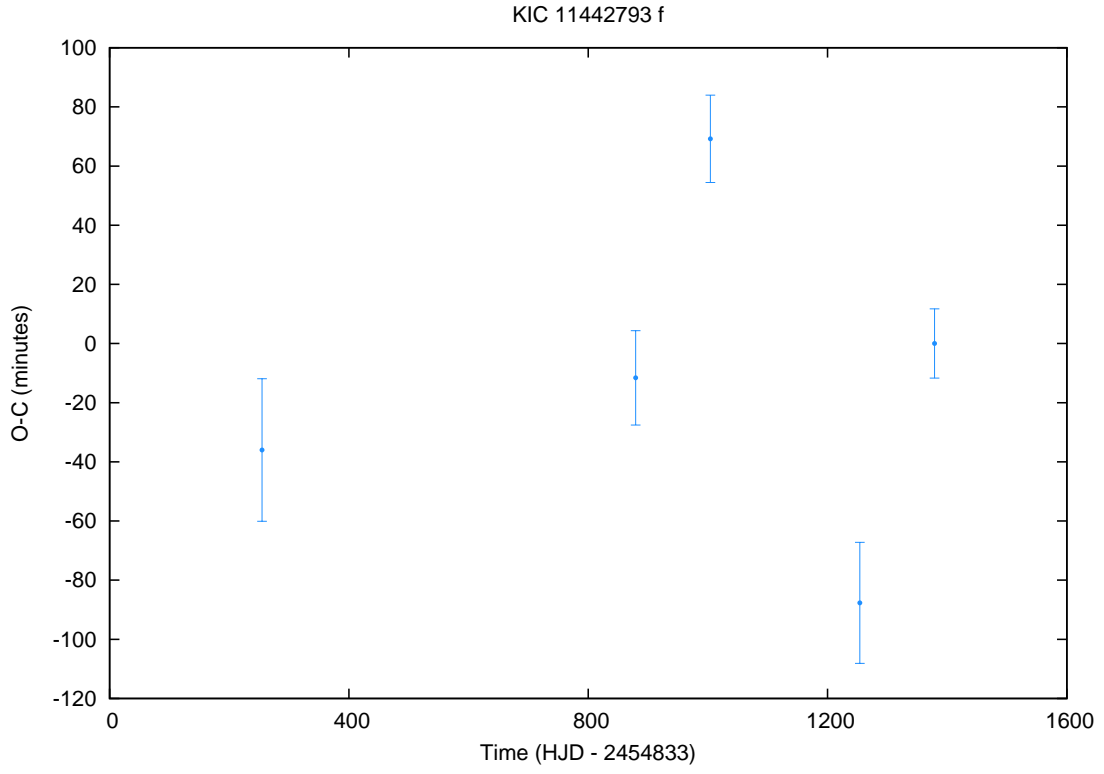


Fig. 14.— Transit timing variations of planet f. Observed mid-times of planetary transits (O) minus calculated linear ephemeris (C) are plotted with 1σ uncertainties.

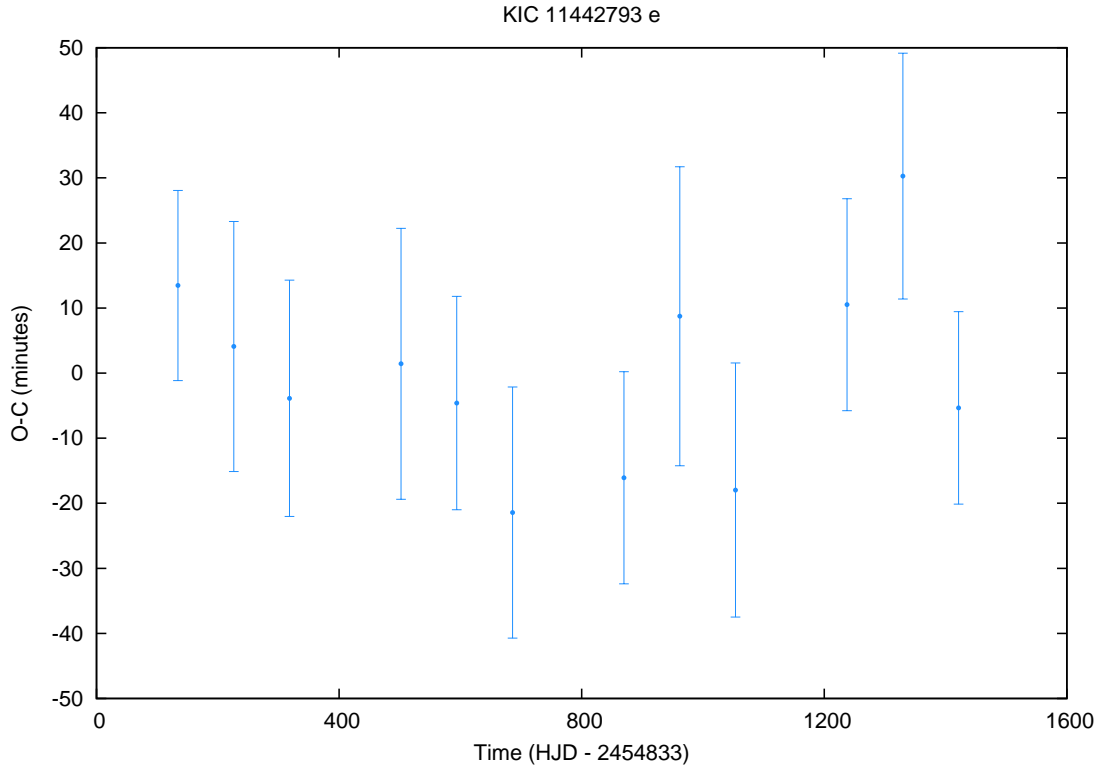


Fig. 15.— Transit timing variations of planet e. Observed mid-times of planetary transits (O) minus calculated linear ephemeris (C) are plotted with 1σ uncertainties.

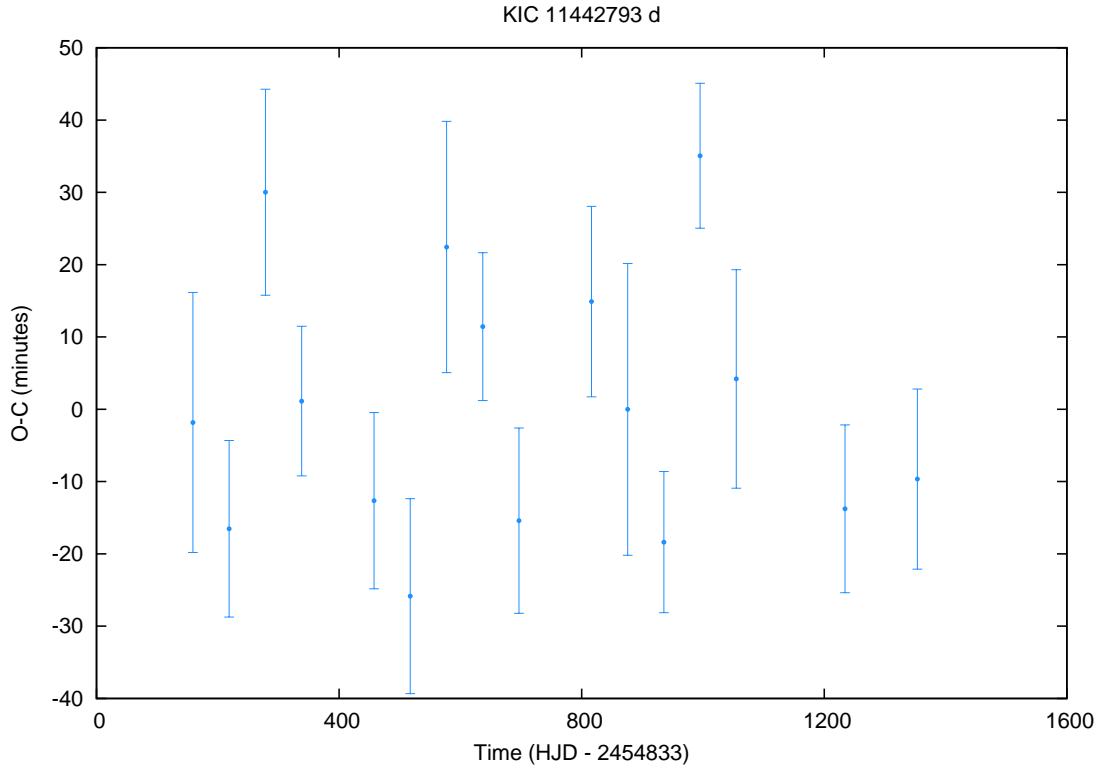


Fig. 16.— Transit timing variations of planet d. Observed mid-times of planetary transits (O) minus calculated linear ephemeris (C) are plotted with 1σ uncertainties.

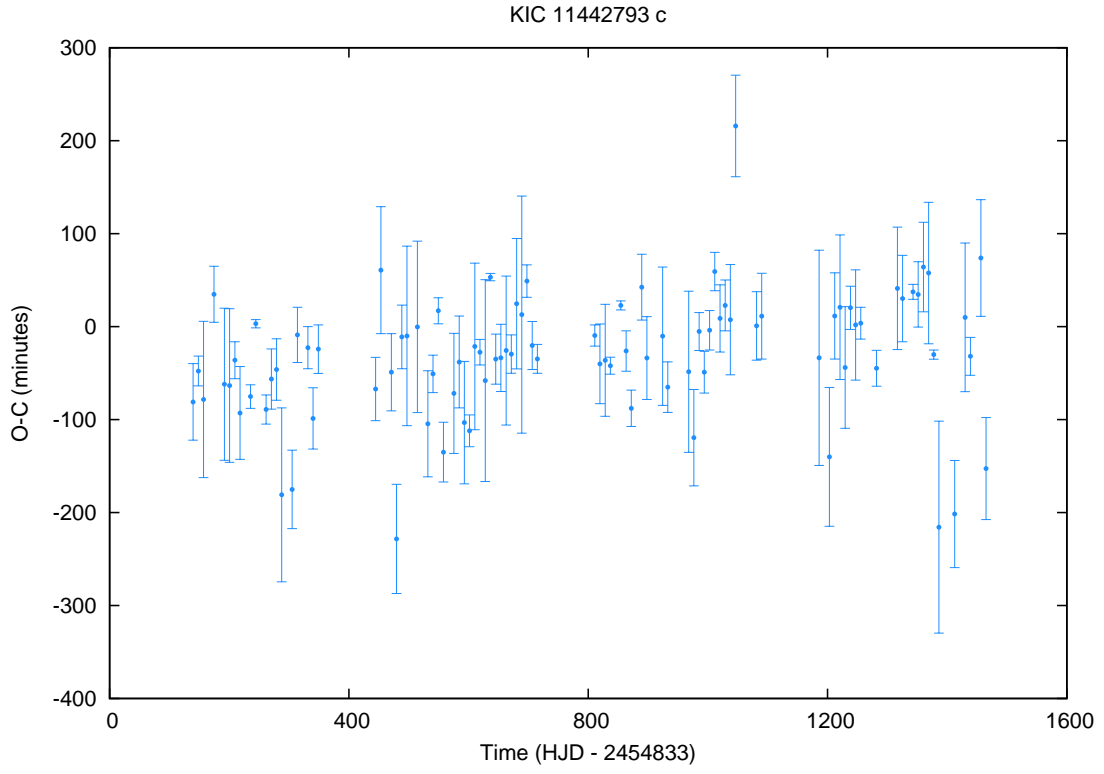


Fig. 17.— Transit timing variations of planet c. Observed mid-times of planetary transits (O) minus calculated linear ephemeris (C) are plotted with 1σ uncertainties.

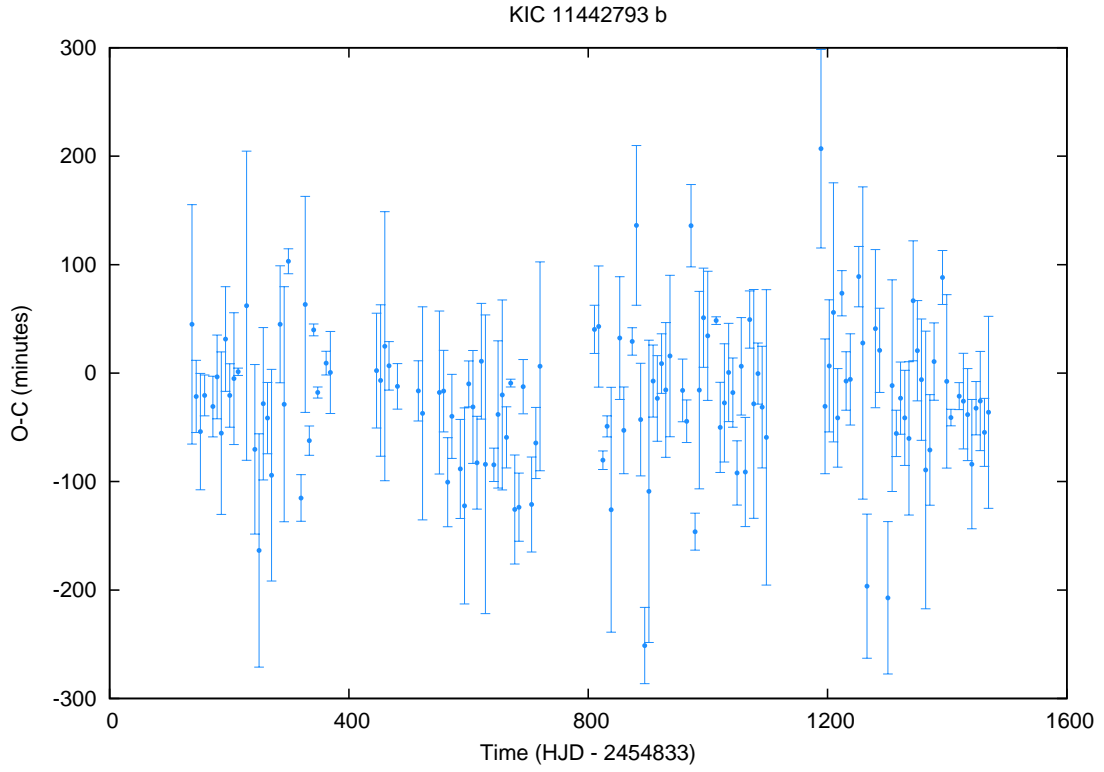


Fig. 18.— Transit timing variations of planet b. Observed mid-times of planetary transits (O) minus calculated linear ephemeris (C) are plotted with 1σ uncertainties.

rough estimate stable orbits for the outer pair should exist up to $e \sim 0.1$. The grey region where an overlapping occurs between aphelion from an inner planet and the perihelion from the outer planet is 'dangerous' due to possible close encounters.

The picture changes when a more detailed systematic numerical investigation of up to 10 Gyrs is performed taking into account all five outer planets (the exclusion of the innermost pair b-c for the integration of the equations of motion is justified because of the large Hill radii between planet e and planet d). For an initial grid of $0.0 \leq e_h \leq 0.04$ and $0.021 \leq e_g \leq 0.05$ we show the respective stability plot in Fig. 20. The stability measure was the dynamical evolution of the eccentricity of planet g. A regular behaviour over the whole integration time was a guarantee for the stability of the whole system; irregular behaviour as sign of chaoticity of the orbit always lead to unstable motion of the whole system sooner or later (sometimes only after several 10^6 years as some integrations have shown). As result we found that initial eccentricities inside the blue region in this plot to the lower left corner and inside the two black lines, lead to stable motion over the whole integration time. Initial conditions chosen outside this region lead to chaotic motion and finally to an unstable system. Long term integrations up to 10 Gyrs for larger masses of the planets (1.05, 1.1, 1.15, 1.2, 1.25 .. times the estimated masses) lead to stable motion with arbitraly chosen initial conditions well inside the stable zone (red point in Fig. 20; $e_h = 0.015$ and $e_g = 0.028$) up to masses 1.2 times larger than the estimated ones. **We estimate the masses of the planets considering their sizes and assuming representative mean densities for each planetary class (gas giants, ice giants, large and small super-Earths). The values assumed are 0.8 Jupiter masses for planet h, 1.7 Neptune masses for planet g, 10 Earth masses for planets f, e, and d, and 3 Earth masses for planets c and b.**

Consequently the uncertainty of the masses involved should not change the picture

significantly for slightly larger masses involved. We conclude that KIC 11442793, from a dynamical point of view, is an interesting 7-planet system where the cited **secular resonances** do not really play an important role. Its stability is determined primarily from the stability of the two outer planets h and g as has been shown here.

7. Formation and evolution of the system

Models of planet formation include theories about planet-planet scattering followed by tidal circularization (Rasio & Ford 1996; Lin & Ida 1997; Chatterjee et al. 2008; Beaugé & Nesvorný 2012). Another possible mechanism of planet formation builds planets at relative large distances of the star and later these planets migrate inwards through a disk (Goldreich & Tremaine 1980; Lin et al. 1996; Ward 1997; Murray et al. 1998). The first mechanism does not likely form compact multiple systems such the ones observed by *Kepler* (Batalha et al. 2013), characterized by being compact and by having low relative inclination orbits (Fang & Margot 2012; Tremaine & Dong 2012). Different mechanisms have been proposed to explain the origin of the latter systems. One promising possibility is in-situ formation, see for example (Chiang & Laughlin 2013; Chatterjee & Tan 2013), including the observed feature that many of those systems have planets orbiting close to, but not exactly at, mean motion resonances (Lithwick & Wu 2012; Petrovich et al. 2013).

We show in Fig. 21 a schematic view of the periods and relative sizes of 8 multiple transiting planetary systems discovered by *Kepler* with 5 transiting planets or more, together with the planetary system reported in this paper. There are also multiple systems discovered by radial velocity hosting 6 or more planets, like GJ 667C (Anglada-Escudé et al. 2013), HD 40307 (Tuomi et al. 2013), or HD 10180 (Lovis et al. 2011). But their orbital properties and even their existence is not as secure as those of transiting candidates. For example, consider the case of the system GJ 581 (Hatzes 2013) or the discussion in the

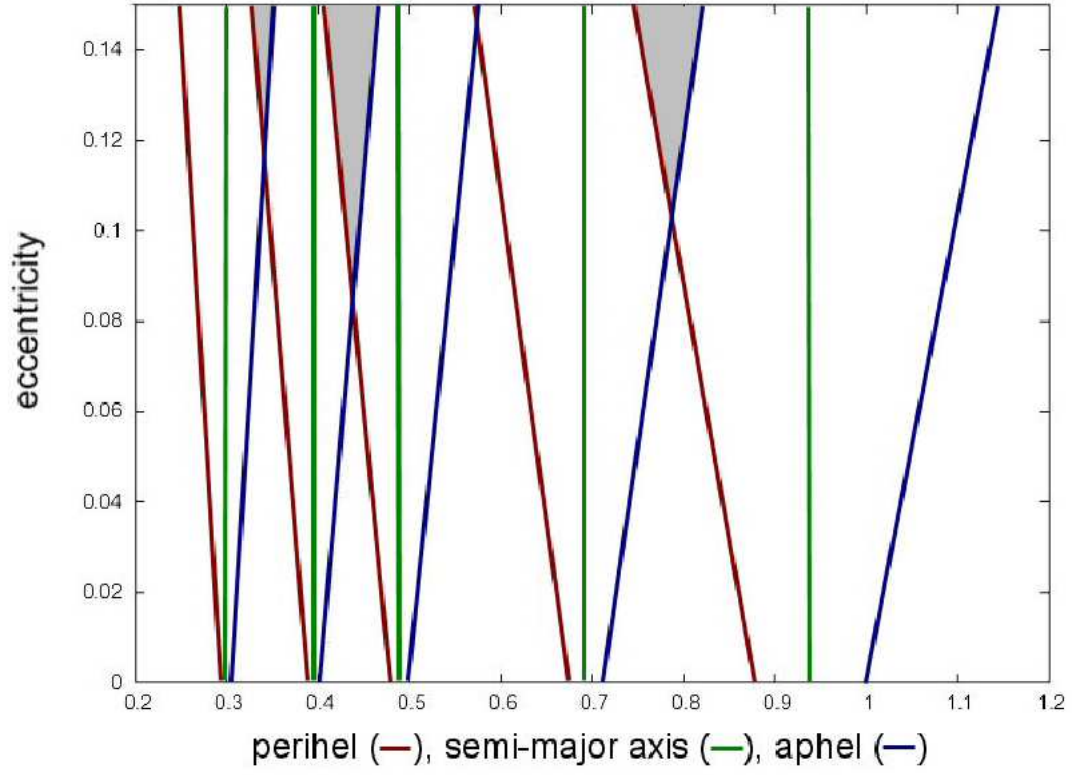


Fig. 19.— An estimate of the overlapping regions (grey) of the orbits of the five outer planets based on the assumed eccentricity.

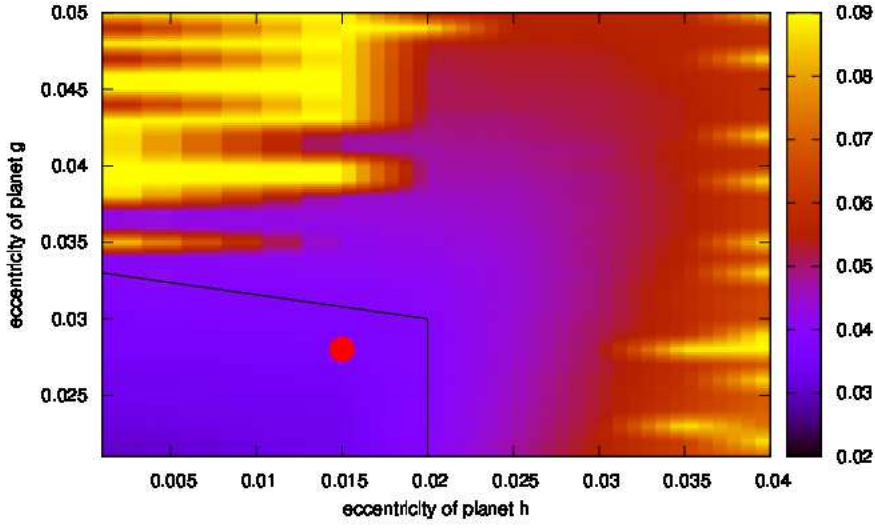


Fig. 20.— Stability plot e_g versus e_h : initial values outside the blue region limited by the thick lines lead to unstable motion and consequently to a decay of the planetary system. The stability measure was the eccentricity of planet h. Long-term low values of this eccentricity guarantee the stability of the system during our integrations, while higher values lead to chaotic motion and instability (see text). The red point served as initial conditions for models with larger masses involved.

literature if HD 10180 is orbited by six (Feroz et al. 2011), seven (Lovis et al. 2011), or even nine (Tuomi 2012) planets. Therefore, we limit ourselves in Fig. 21 to the discussion of multiple transiting systems. Among the systems shown, KIC 11442973 presented here is the only one showing a clear hierarchy, like our Solar System, and the only one to host a giant planet larger than 10 Earth radii. **Such systems are typically more difficult to form because giant planets tend to excite the eccentricity of less massive planets during the migration processes, compromising the long term stability of the system (see, for example, Raymond et al. 2008).** Note that there are two additional known systems hosting simultaneously super-Earths and gas giants, but these two systems orbit M dwarfs, and only the second example is a compact system. GJ 676A (Anglada-Escudé & Tuomi 2012) hosts up to 4 planets, including one super-Earth in a 3.6 days orbit and one 5 Jupiter masses planet in a 1050 days orbit. GJ 876 (Rivera et al. 2010) is also an M-dwarf hosting one super-Earth of 6 Earth masses at 1.9 days orbital period, a 0.7 Jupiter masses planet at 20 days, a 2.3 Jupiter masses planet at 61 days, and a 14 Earth masses planet in a 124 days orbit. However, KIC 11442793 is a late F/early G solar-like star, hosting a more complex system where dynamical interactions play an important role in the long term stability of the system.

7.1. About the possible existence of moons in the planetary system

We have discussed in previous sections the possibility that KIC 11442793g hosts a moon. Figure 11 shows that the transit epochs 1, 2 and 3 show features morphologically equivalent to an exomoon orbiting the planet (Sartoretti & Schneider 1999; Szabó et al. 2006; Kipping 2011). However, considering the distance between the transit epoch 3 and the moon-like event marked with an arrow in Figure 11, the estimated projected distance between the planet and the exomoon candidate would be orbiting close to the Hill radius of

the planet, which is too far away to guarantee the long term stability of the satellite, usually limited to a distance of one third (Barnes & O’Brien 2002) to one half (Domingos et al. 2006) of the planetary Hill sphere. With the current data set, we cannot exclude that the event marked with an arrow in Figure 11 is caused by instrumental residuals. However, the distorted shape features of transits 1 and 2 cannot be explained simply by the impact of stellar activity and their origin remains unclear. Space surveys have regularly been used to rule out the presence of moons around extrasolar planets (Pont et al. 2007; Deeg et al. 2010). So far, the most extensive search for exomoons (Kipping et al. 2012) has taken the advantage of the simultaneous change in the transit timing and transit duration changes produced by the hypothetical satellites (Kipping 2009a,b). However, until now only negative results have been reported (Kipping et al. 2013b,a). A possible reason for this lack of success is that searches have been limited to isolated, typically giant planets. However, if these systems are formed by planet-planet scattering, they are unlikely to maintain the moons during their formation process (Gong et al. 2013). In turn, migration tends to remove moons from planetary systems (Namouni 2010). Therefore, in-situ formed compact systems could be more prone to host exomoons in long timescales.

8. Summary

We report the discovery of a planetary system with seven transiting planets with orbital periods in the range from 7 to 330 days (0.074 to 1.01 AU). The system is hierarchical, the two innermost planets have sizes close to Earth and their period ratio is within 0.5% of the 4:5 mean motion resonance. The three following planets are super-Earths with sizes between 2 and 3 Earth radii whose periods are close to a 2:3:4 chain. From the observational data set we cannot determine their masses or the value of their mean longitudes, but the ratio of their mean motions is close to a Laplace resonance. The outermost planets are

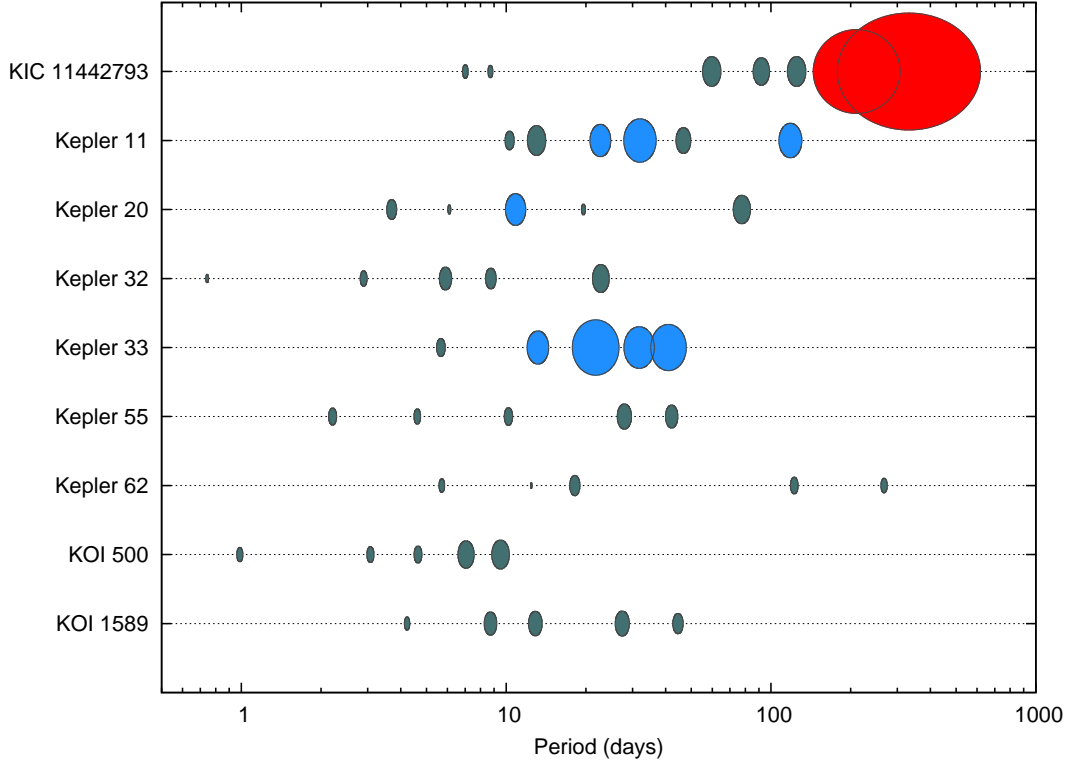


Fig. 21.— Comparison of different multiple systems. Kepler-11 (Lissauer et al. 2011a), Kepler-20 (Gautier et al. 2012; Fressin et al. 2012), Kepler-32 (Fabrycky et al. 2012), Kepler-33 (Lissauer et al. 2012), Kepler-55 (Steffen et al. 2013), Kepler-62 (Borucki et al. 2013), KOI-500 (Xie 2012; Wu & Lithwick 2012), KOI-1589 (Xie 2012; Wu & Lithwick 2012). Color codes separate Earth and Super-Earth planets (up to 4 Earth radii, shown in green), Neptune-sized planets (between 4 and 8 Earth radii, shown in blue), and gas giants (larger than 8 Earth radii, shown in red).

two gas giants at distances of 0.7 and 1.0 AU. There are other systems of super-Earths, discovered either by radial velocity or by transit, which show some similarities, for example GJ 876 (Rivera et al. 2010) or KOI 152 (Wang et al. 2012), but these systems only contain super-Earths, while KIC 11442793 is a hierarchical system. As a singularity among the other multiple systems found by *Kepler* or radial velocity, KIC 11442793 contains a gas giant planet similar to Jupiter orbiting at 1 AU. Systems with super-Earths close to a Laplace resonance are also believed to be frequent (Chiang & Laughlin 2013), but this particular system poses new challenges due to the presence of the gas giants g and h, which have the most intense gravitational interaction measured among extrasolar planets so far (25.7 h of change in the ephemeris). If *Kepler* cannot continue the follow up of this system (Cowen 2013), the follow-up of the Earth and super-Earth planets of this system will be challenging in the near future, as they are beyond reach for CHEOPS (Broeg et al. 2013) or TESS (Ricker et al. 2010). Only PLATO (Rauer & Catala 2011) will be able to study in detail their evolution. However, the gas giants g and f produce 0.5% and 0.8% transits, which should be observable from ground, which makes of this system an attractive target for future follow-up studies.

We are grateful to É. Bálint, Ph. von Paris and M. Godolt for useful discussions concerning this paper. This paper includes data collected by the *Kepler* mission. Funding for the *Kepler* mission is provided by the NASA Science Mission directorate. Some/all of the data presented in this paper were obtained from the Mikulski Archive for Space Telescopes (MAST). STScI is operated by the Association of Universities for Research in Astronomy, Inc., under NASA contract NAS5-26555. Support for MAST for non-HST data is provided by the NASA Office of Space Science via grant NNX09AF08G and by other grants and contracts.

REFERENCES

- Anglada-Escudé, G., & Tuomi, M. 2012, *A&A*, 548, A58
- Anglada-Escudé, G., Tuomi, M., Gerlach, E., et al. 2013, ArXiv e-prints, arXiv:1306.6074
- Baglin, A., Auvergne, M., Boissard, L., et al. 2006, in COSPAR, Plenary Meeting, Vol. 36, 36th COSPAR Scientific Assembly, 3749
- Barnes, J. W., & O’Brien, D. P. 2002, *ApJ*, 575, 1087
- Batalha, N. M., Rowe, J. F., Gilliland, R. L., et al. 2010, *ApJ*, 713, L103
- Batalha, N. M., Rowe, J. F., Bryson, S. T., et al. 2013, *ApJS*, 204, 24
- Beaugé, C., & Nesvorný, D. 2012, *ApJ*, 751, 119
- Borucki, W. J., Koch, D., Basri, G., et al. 2010, *Science*, 327, 977
- Borucki, W. J., Agol, E., Fressin, F., et al. 2013, *Science*, 340, 587
- Broeg, C., Fortier, A., Ehrenreich, D., et al. 2013, in European Physical Journal Web of Conferences, Vol. 47, European Physical Journal Web of Conferences, 3005
- Cabrera, J. 2010, in EAS Publications Series, Vol. 42, EAS Publications Series, ed. K. Goździewski, A. Niedzielski, & J. Schneider, 109–116
- Cabrera, J., Csizmadia, S., Erikson, A., Rauer, H., & Kirste, S. 2012, *A&A*, 548, A44
- Chambers, J. E. 1999, *MNRAS*, 304, 793
- Chaplin, W. J., Sanchis-Ojeda, R., Campante, T. L., et al. 2013, *ApJ*, 766, 101
- Chatterjee, S., Ford, E. B., Matsumura, S., & Rasio, F. A. 2008, *ApJ*, 686, 580
- Chatterjee, S., & Tan, J. C. 2013, ArXiv e-prints, arXiv:1306.0576

- Chiang, E., & Laughlin, G. 2013, MNRAS, 431, 3444
- Cowen, R. 2013, Nature, 497, 417
- Csizmadia, S., Pasternacki, T., Dreyer, C., et al. 2013, A&A, 549, A9
- Csizmadia, S., Moutou, C., Deleuil, M., et al. 2011, A&A, 531, A41
- Cutri, R. M., Skrutskie, M. F., van Dyk, S., et al. 2003, 2MASS All Sky Catalog of point sources.
- Deeg, H. J., Moutou, C., Erikson, A., et al. 2010, Nature, 464, 384
- Domingos, R. C., Winter, O. C., & Yokoyama, T. 2006, MNRAS, 373, 1227
- Fabrycky, D. C., Ford, E. B., Steffen, J. H., et al. 2012, ApJ, 750, 114
- Fang, J., & Margot, J.-L. 2012, ApJ, 761, 92
- Feroz, F., Balan, S. T., & Hobson, M. P. 2011, MNRAS, 415, 3462
- Ford, E. B., & Gaudi, B. S. 2006, ApJ, 652, L137
- Ford, E. B., Rowe, J. F., Fabrycky, D. C., et al. 2011, ApJS, 197, 2
- Ford, E. B., Fabrycky, D. C., Steffen, J. H., et al. 2012a, ApJ, 750, 113
- Ford, E. B., Ragozzine, D., Rowe, J. F., et al. 2012b, ApJ, 756, 185
- Fressin, F., Torres, G., Rowe, J. F., et al. 2012, Nature, 482, 195
- Gandolfi, D., Alcalá, J. M., Leccia, S., et al. 2008, ApJ, 687, 1303
- Gautier, III, T. N., Charbonneau, D., Rowe, J. F., et al. 2012, ApJ, 749, 15
- Geem, Z. G., Kim, J. H., & Loganathan, G. V. 2001, Simulation, 76, 60,
<http://sim.sagepub.com/cgi/content/abstract/76/2/60>

- Giménez, A. 2006, *A&A*, 450, 1231
- Goldreich, P., & Tremaine, S. 1980, *ApJ*, 241, 425
- Gong, Y.-X., Zhou, J.-L., Xie, J.-W., & Wu, X.-M. 2013, *ApJ*, 769, L14
- Gray, D. F. 2005, *The Observation and Analysis of Stellar Photospheres*
- Hatzes, A. P. 2013, *Astronomische Nachrichten*, 334, 616
- Hauschildt, P. H., Allard, F., & Baron, E. 1999, *ApJ*, 512, 377
- Holman, M. J., & Murray, N. W. 2005, *Science*, 307, 1288
- Huang, X., Bakos, G. Á., & Hartman, J. D. 2013, *MNRAS*, 429, 2001
- Kipping, D. M. 2009a, *MNRAS*, 392, 181
- . 2009b, *MNRAS*, 396, 1797
- . 2011, *MNRAS*, 416, 689
- Kipping, D. M., Bakos, G. Á., Buchhave, L., Nesvorný, D., & Schmitt, A. 2012, *ApJ*, 750, 115
- Kipping, D. M., Forgan, D., Hartman, J., et al. 2013a, *ArXiv e-prints*, arXiv:1306.1530
- Kipping, D. M., Hartman, J., Buchhave, L. A., et al. 2013b, *ApJ*, 770, 101
- Léger, A., Rouan, D., Schneider, J., et al. 2009, *A&A*, 506, 287
- Lehmann, H., Tkachenko, A., Semaan, T., et al. 2011, *A&A*, 526, A124
- Lin, D. N. C., Bodenheimer, P., & Richardson, D. C. 1996, *Nature*, 380, 606
- Lin, D. N. C., & Ida, S. 1997, *ApJ*, 477, 781

- Lissauer, J. J., Fabrycky, D. C., Ford, E. B., et al. 2011a, *Nature*, 470, 53
- Lissauer, J. J., Ragozzine, D., Fabrycky, D. C., et al. 2011b, *ApJS*, 197, 8
- Lissauer, J. J., Marcy, G. W., Rowe, J. F., et al. 2012, *ApJ*, 750, 112
- Lithwick, Y., & Wu, Y. 2012, *ApJ*, 756, L11
- Lithwick, Y., Xie, J., & Wu, Y. 2012, *ApJ*, 761, 122
- Lovis, C., Ségransan, D., Mayor, M., et al. 2011, *A&A*, 528, A112
- Mandel, K., & Agol, E. 2002, *ApJ*, 580, L171
- Mazeh, T., Nachmani, G., Holczer, T., et al. 2013, *ArXiv e-prints*, arXiv:1301.5499
- Murray, N., Hansen, B., Holman, M., & Tremaine, S. 1998, *Science*, 279, 69
- Namouni, F. 2010, *ApJ*, 719, L145
- Nesvorny, D., Kipping, D., Terrell, D., et al. 2013, *ArXiv e-prints*, arXiv:1304.4283
- Ofir, A., & Dreizler, S. 2012, *ArXiv e-prints* 1206.5347, arXiv:1206.5347
- Petrovich, C., Malhotra, R., & Tremaine, S. 2013, *ApJ*, 770, 24
- Pont, F., Gilliland, R. L., Moutou, C., et al. 2007, *A&A*, 476, 1347
- Rasio, F. A., & Ford, E. B. 1996, *Science*, 274, 954
- Rauer, H., & Catala, C. 2011, in *IAU Symposium*, Vol. 276, *IAU Symposium*, ed. A. Sozzetti, M. G. Lattanzi, & A. P. Boss, 354–358
- Raymond, S. N., Barnes, R., & Mandell, A. M. 2008, *MNRAS*, 384, 663

- Ricker, G. R., Latham, D. W., Vanderspek, R. K., et al. 2010, in *Bulletin of the American Astronomical Society*, Vol. 42, American Astronomical Society Meeting Abstracts 215, 450.06
- Rivera, E. J., Laughlin, G., Butler, R. P., et al. 2010, *ApJ*, 719, 890
- Sartoretti, P., & Schneider, J. 1999, *A&AS*, 134, 553
- Shulyak, D., Tsymbal, V., Ryabchikova, T., Stütz, C., & Weiss, W. W. 2004, *A&A*, 428, 993
- Steffen, J. H., Fabrycky, D. C., Ford, E. B., et al. 2012a, *MNRAS*, 421, 2342
- Steffen, J. H., Ford, E. B., Rowe, J. F., et al. 2012b, *ApJ*, 756, 186
- Steffen, J. H., Fabrycky, D. C., Agol, E., et al. 2013, *MNRAS*, 428, 1077
- Szabó, G. M., Szatmáry, K., Divéki, Z., & Simon, A. 2006, *A&A*, 450, 395
- Tenenbaum, P., Jenkins, J. M., Seader, S., et al. 2013, *ApJS*, 206, 5
- Tremaine, S., & Dong, S. 2012, *AJ*, 143, 94
- Tsymbal, V. 1996, in *Astronomical Society of the Pacific Conference Series*, Vol. 108, M.A.S.S., *Model Atmospheres and Spectrum Synthesis*, ed. S. J. Adelman, F. Kupka, & W. W. Weiss, 198
- Tuomi, M. 2012, *A&A*, 543, A52
- Tuomi, M., Anglada-Escudé, G., Gerlach, E., et al. 2013, *A&A*, 549, A48
- Wang, S., Ji, J., & Zhou, J.-L. 2012, *ApJ*, 753, 170
- Ward, W. R. 1997, *Icarus*, 126, 261

Wright, E. L., Eisenhardt, P. R. M., Mainzer, A. K., et al. 2010, *AJ*, 140, 1868

Wu, Y., & Lithwick, Y. 2012, ArXiv e-prints, arXiv:1210.7810

Xie, J.-W. 2012, ArXiv e-prints, arXiv:1208.3312